Focusing properties of mosaic crystals

M. Sánchez del Río[a], M. Gambaccini[b], G. Pareschi[c], A. Taibi[b], A. Tuffanelli[b], and A. Freund[a]

[a]European Synchrotron Radiation Facility
BP 220, 38043 Grenoble-Cedex, France

[b]Dipartimento di Fisica, Università di Ferrara and INFN sezione di Ferrara
Via Paradiso 12, I-44100 Ferrara, Italy

[c]Danish Space Research Institute
Juliane Mariies Vej 30, 2100 Copenhagen, Denmark

ABSTRACT

X-ray instruments with mosaic crystals are proposed and used in many applications in synchrotron radiation, medical physics and astrophysics. These crystals present a parafocusing of the x-ray beam in the diffraction plane, which is thoroughly analyzed in this paper. We studied the evolution of the cross section of the diffracted beam, using several samples of Highly Oriented Pyrolythic Graphite crystals coming from different suppliers. The experiment has been performed at the European Synchrotron Radiation Facility (beamline BM5). The results clearly show a parafocusing effect in the 1:1 magnification ratio along the diffraction plane and a defocusing effect along the perpendicular plane. The secondary extinction coefficient is also measured.

Keywords: Mosaic crystals, Highly Oriented Pyrolytic Graphite (HOPG), x-ray focusing, secondary extinction

1. INTRODUCTION

Mosaic crystals provide an interesting choice for medical physics[1,2] (quasi-monochromatic x-rays for mammography), astrophysics applications[3,4] (polarimeters and hard x-ray concentrators), neutron monochromators, analyzers and filters; and x-ray monochromators for synchrotron radiation.[5,6] Mosaic crystals are considered to be formed by a large number of small perfect crystallites of microscopical or submicroscopical size which are oriented almost but not exactly, parallel to one another. They show a much wider but lower diffraction profile as compared to perfect crystals. These diffraction profiles can be calculated using the theory in Ref. 7 or in Ref. 8 which are equivalent. They assume that the crystallites are oriented almost parallel to the crystal surface (for Bragg case) following a Gaussian distribution which full-width-at-half-maximum (FWHM) τ is considered the mosaic spread or mosaicity. It has been found experimentally that the reflectivity profiles of real Highly Oriented Pyrolytic Graphite (HOPG) do agree only roughly with the theory predictions. Moreover, the diffraction profiles recorded using highly collimated narrow beams (of micrometrical size) are very irregular, suggesting that the structure of the real mosaic crystals is much more complex than the assumptions in the theoretical models. It was suggested[9] that the HOPG could be considered as a "supermosaic" structure, consisting of crystallites grouped to form blocks or layers which are independent from one to another. Detailed measurements of rocking curves as a function of the crystal depth[10] showed that the HOPG can be described by two types of mosaic structures. The first type consists of macrostructures formed by relatively large tiles (about 40 μm-thick parallel to the c-axis and about 400 μm in perpendicular) which are misoriented between them by an average mosaic spread of 0.3°. The second mosaic structure on a smaller scale has a mosaic spread τ around 0.1°. High resolution x-ray topographic investigations[11] produced direct images of these macrostructures and showed the alignment between them. It is worth to note that the structure, dimensions and distribution of the crystallites and macrostructures depend on the different samples, perhaps on the particular zone of the same sample, and specially on the fabrication process. HOPG samples are produced by different companies, namely Advanced Ceramics (USA), Optigraph (Russia) and Panasonic (Japan). The studies already mentioned were done using samples from Advanced Ceramics. Different results could be expected from samples from other manufacturers, which use different fabrication methods. Thus, systematic topographic and diffraction studies on a wide collection of samples from different origins are desirable to gain information on the mosaic crystals and to understand the microstructure of HOPG.

Other author information: (Send correspondence to M.S.R)
M.S.R: Email: srio@esrf.fr; Telephone: +33-476 882 513; Fax: +33-476 882 160

In this work we will study imaging properties of these crystals that depend on the mosaic microstructure. It is well known that the crystallites inside a flat mosaic crystal produce an interesting parafocusing effect (see, for instance, Ref. 12) of the x-ray beam in the diffraction plane in a 1:1 magnification configuration. That means that a flat mosaic crystal focuses *monochromatic* light in the diffraction plane when the distances source-to-crystal and crystal-to-image are equal (see Fig. 1). On the other hand, a defocusing effect is produced in the plane perpendicular to the diffraction plane. As a consequence, the image of a point source after diffraction by a mosaic crystal is a segment in direction perpendicular to the diffraction plane. In addition, the position of the focal spot in the diffraction plane depends on the Bragg angle (thus on the photon energy) producing spots in different spatial positions for different photon energies. This produces a smearing effect of the image spot when a polychromatic x-ray source is used. This focusing effect depends on the photon energy is often called parafocusing or pseudofocusing or even chromatic aberration in the focalization. The focal spot is also broaded if one considers that the diffraction takes place in the crystal bulk and not only on the surface. All these effects can be considered in a ray-tracing program[13] to simulate focal spots produced by ideal mosaic crystals.

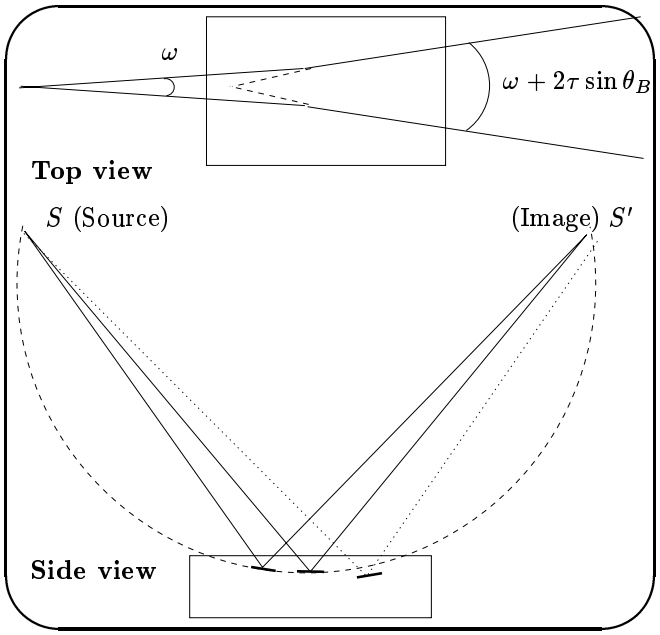

Figure 1. *Top:* Defocusing effect of mosaic crystals in the plane perpendicular to the diffraction plane. The beam divergence is increased in $2\tau \sin\theta_B$ due to crystal mosaicity.
Bottom: Parafocusing effect of a mosaic crystal in the diffraction plane: Several rays with the same energy coming from the source point S are diffracted by different crystallites inside the mosaic crystal according to Bragg's law. This requires that the ray has to travel inside the crystal until it finds a crystallite with the correct orientation. The diffracted rays converge to a point S' (assuming that the penetration depth and footprint on the crystal are distances much smaller than the source-crystal distance). The crystal-S' distance is equal to the S-crystal distance thus the parafocusing effect happens in a magnification ratio 1:1. When another ray (dotted) with the same energy encounters a crystallite deeper in the crystal, it is reflected to a point close but different from S', producing a broadening in the focal spot due to the penetration of the beam inside the crystal bulk. The same concept could be applied to rays of a different energy, but clearly they will be focused to another different point, due to the fact that the Bragg angle is different. The parafocusing effect can also be understood as produced by crystallites that follow a curved surface (dashed circle), like a spherical mirror. The crystallite orientation must follow the Rowland circle to assure that the Bragg law will be fulfilled. Therefore, the 1:1 magnification geometry is just a consequence of the Rowland condition.

It is obvious that in real life the results can be different from the theoretical simulations because of the lack of perfectness and macrostructures of the mosaic crystals. The focusing properties of HOPG crystals are thoroughly studied in this paper, confirming experimentally the parafocusing effect. The evolution of the beam size after diffraction by HOPG crystals has been recorded and images of the beam cross section in both the diffraction plane

and the perpendicular plane are presented as a function of the distance to the crystal.

The parafocusing properties affect the image quality in mammographic applications[14] and influence the imaging properties of Bragg telescopes for off-axis photon beams together with polarimetric performances.[15] Imaging investigations of the HOPG crystals can also give complementary information to other methods in order to determine the macrostructures of the mosaic crystals. The parafocusing effect can also be exploited in spectroscopic experiments to collect and concentrate photons produced from a target irradiated with x-rays.[12]

2. EXPERIMENTAL

Experiments were carried out at the beamline BM5 at the ESRF. A schematic setup of the experiment is shown in Fig. 2. The source was a bending magnet with a critical energy of 20 keV. The beamline was equipped with a double crystal $Si < 1,1,1 >$ monochromator, placed at 30 m from the source. The first crystal of the monochromator was flat and the second crystal was either flat or sagittally bent, in order to focus in the horizontal plane. The sample was mounted at 40 m from the source on a 3-axes diffractometer using the horizontal plane as diffracting plane. Rocking curves were measured using a Si diode detector. Beam cross sections were imaged using both high resolution films and a position-sensitive digital detector. Aluminium filters of different thicknesses were used to attenuate the beam to match the dynamic range of the detectors. The digital detector was based on a direct deposition of a gadolinium oxysulphide powder onto a CCD surface. The CCD had a pixel pitch of 22.5 μm and 770x1152 pixels. All CCD operations were driven by means of an electronic unit which provided slow-scan readout and inverted mode operation for dark current reduction. The analog signal was digitized by means of a 12-bits data acquisition board. The evaluation of the phosphor-coated CCD showed high spatial resolution performance.[16,17]

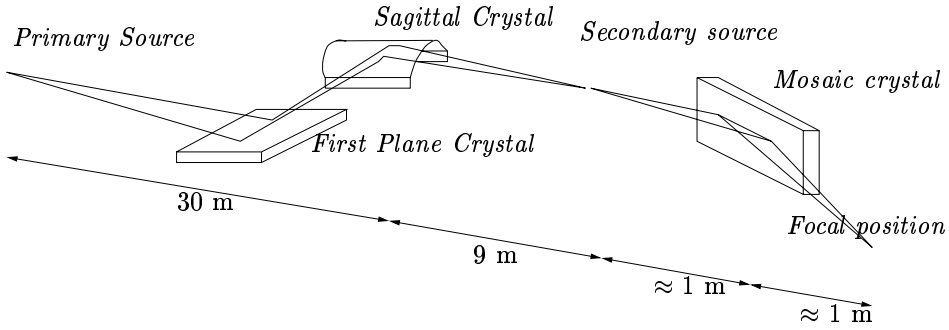

Figure 2. Schematic draw of the experimental setup in when using a secondary source.

Most of the experimental data have been recorded using a HOPG sample manufactured by Optigraph selected from a collection of several samples. The selection criterion was the uniformity of the rocking curves measured at different positions along the crystal surface (Fig. 3). Rocking curves of the HOPG reflection (0,0,2) were measured at a photon energy of 18 keV. Their width were compared with diffraction profiles calculated using the XOP software[18] that codes the theory of Zachariasen. Other three samples manufactured by Advanced Ceramics (grade ZYA), Panasonic and Optigraph were also used. The main parameters of all the used samples are in Table 1.

Beam cross sections were measured in two beamline configurations: using either a flat or a bent second crystal of the monochromator. In the first case the mosaic crystal sees the source (the bending magnet) at 40 m upstream from it. The monochromator selects the proper energy but not focusing is done. The bending magnet source will be referred hereafter as *primary source*. The mosaic crystal would image the primary source and produce a focus at the same distance downstream from it. However, this is not expected because in order to obtain parafocusing the divergence of the beam impinging on the mosaic crystal should be of the same order or bigger than the mosaicity. The beam divergence is defined by the ratio between the slit used before the mosaic (about 1 mm) and the distance (40 m), thus about 25 μrad. This is comparable with the Darwin width of a single crystallite. In this configuration, we measured the evolution of the beam at distances up to 3.5 m downstream from the mosaic crystal.

In order to be able to observe the 1:1 magnification focusing effect of the mosaic crystals, we need a divergent source close to the sample. To this aim we created a *secondary source* produced by focusing the bending magnet source onto a line placed about one meter upstream from the mosaic crystal. For that purpose, a sagittally bent $Si < 1,1,1 >$ crystal was placed as second crystal in the monochromator.

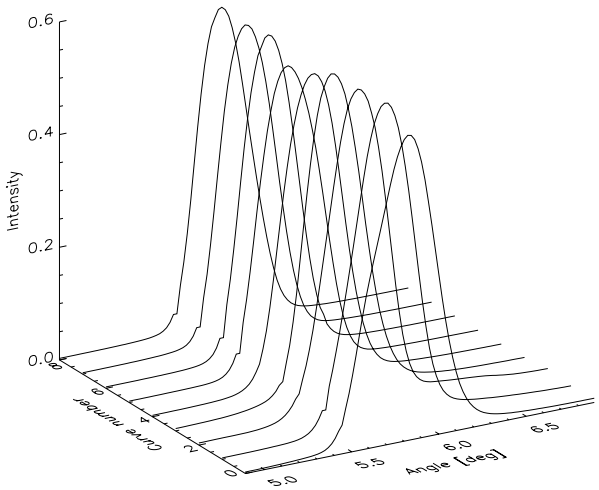

Figure 3. Diffraction profiles of the Optigraph sample (1 mm thick) at 18 keV. The different curves are taken by illuminating different positions along the crystal length.

Table 1. Parameters of the used samples. The results are from a collection of rocking curves measured at 18 keV using a synchrotron beam after a double crystal $Si < 1,1,1 >$ monochromator and using a slit of 0.2 mm before the mosaic crystal (except for the Panasonic crystal where a 0.5 mm slit was used). The HOPG reflection was (0,0,2). The errors are 1.5 standard deviations of the experimental values. All the angular values are FWHM in degrees. The theoretical values are obtained by calculating the diffracting profile at 18 keV for π polarized radiation (the diffraction plane is horizontal) using the given thickness and a mosaicity τ. The τ value was adjusted in order to obtain a width value close to the experimental one.

Sample/Manufacturer	dimensions [mm]	ω_{exp}	P_{exp}	ω_{theor}	P_{theor}	τ
1 Optigraph	60x28x1.0	0.40±0.04	0.56±0.02	0.41	0.63	0.25
2 Advanced Ceramics	50x10x1.0	0.42±0.06	0.50±0.04	0.42	0.63	0.26
3 Panasonic	20x30x4.0	0.66	0.55	0.65	0.56	0.42
4 Optigraph	60x17x0.5	0.42±0.06	0.50±0.04	0.41	0.59	0.28

The formula that relates the curvature radius to the focal distances is:

$$\frac{1}{f} = \frac{1}{p} + \frac{1}{q} = \frac{2\sin\theta_B}{R_s}. \tag{1}$$

The crystal curvature radius R_s was 1464 mm, the focusing distances were p =30 m, and q =9 m, therefore the monochromator was set to a photon energy of about 18 keV (corresponding to a Bragg angle of θ_B=6.31°) Within this focusing configuration, the divergence of the beam impinging on the mosaic crystal will be Δ=0.32° (calculated from the footprint of the beam on the sagittal crystal which is 5 cm) and the distance to the mosaic crystal (9 m). This value is of the order of the mosaicity, thus we expect to observe the parafocusing effect. With this configuration the theoretical focus (secondary source) is situated at a distance of 1 m upstream from the mosaic crystal. Several images around this focal position of the sagittal crystal were recorded to define exactly the position of the secondary source (Fig. 4). The horizontal focus produced by the sagittal crystal was found experimentally at 96 ± 1 cm upstream from the mosaic crystal. A slit was placed at that position with dimensions 0.08 mm in the horizontal plane and 1.5 mm in vertical, thus producing a vertical line that was the new source for the mosaic crystal.

Some problems were found to find the exact position of the new source (focal image produced by the sagittally bent crystal), due to large depth of focus. In addition, the images recorded (Fig. 4) manifested the existence of two

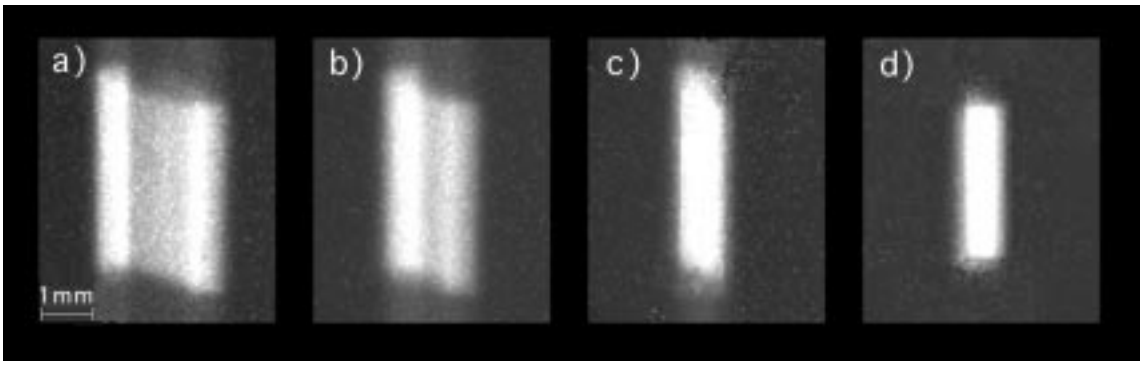

Figure 4. Radiographs of the beam cross section imaged with the digital detector at various distances around the theoretical focal position of the sagittal crystal (secondary source): a) 129 cm, b) 119 cm, c) 105 cm, and d) 96 cm.

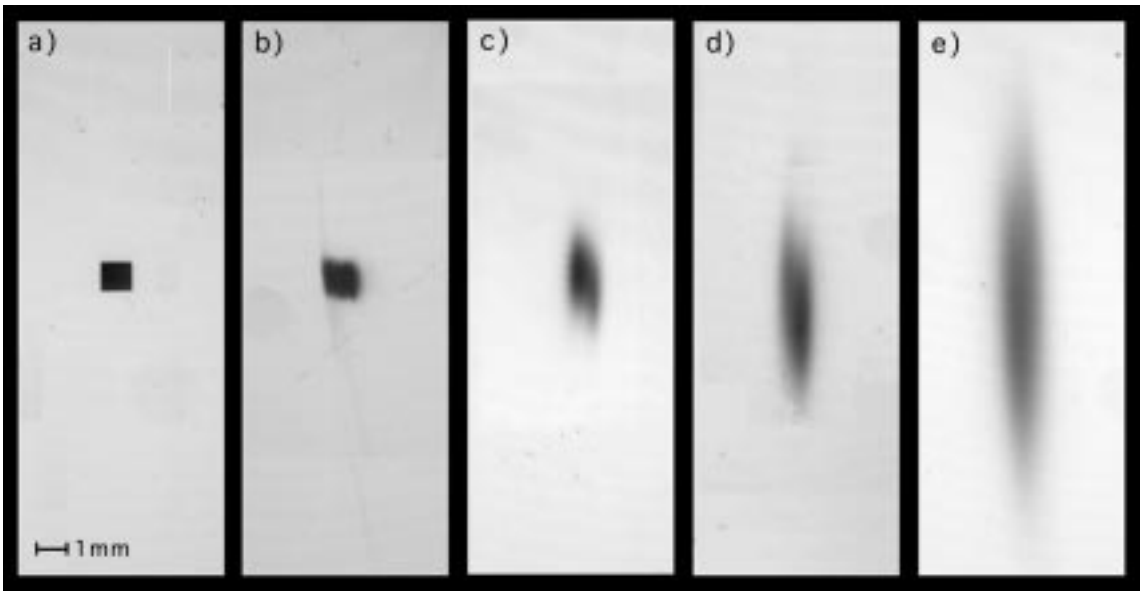

Figure 5. Radiographs of the beam cross section imaged with photographic films. a) image at the mosaic crystal position with the crystal removed. Images after diffraction at several distances downstream from the mosaic crystal: b) 13.5 cm, c) 60 cm, d) 100 cm, e) 200 cm.

regions, separated downstream from the focus and perfectly overlapping at the focus. This effect and its origin will be discussed later.

3. RESULTS AND DISCUSSION

3.1. Beam evolution using the primary source (non-focused beam)

The first experimental configuration used an unfocused incident beam provided by flat monochromator crystals. Therefore, the primary source placed at 40 m upstream from the mosaic crystal was imaged.

Different images have been recorded to study the evolution of the diffracted beam at 8 keV (see Fig. 5). The beam cross section on the mosaic crystal as defined by the entrance slits was 1 x 1 mm^2 . The images were recorded using photographic films placed at different distanced downstream from the mosaic crystal ranging from 55 mm to 3500 mm.

These images show a clearly divergent beam propagation in the vertical plane (perpendicular to the diffraction plane). The expected divergence is about $2\tau \sin\theta_B = 2$ mrad (with $\tau = 0.25^\circ$ and $\theta_B = 13.4^\circ$). The divergence has been calculated by measuring the vertical size of the beam and fitting the data with respect to the crystal-to-film distance. This procedure presents some problems due to the non linearity of the film and different exposition time used, that produces an overestimation of the image spot at long distances. Using images recorded up to 30 cm the divergence resulting from the fit is about 2.6 mrad. Using distances up to 200 cm the resulting divergence is larger.

The beam cross section images in the horizontal plane (diffraction plane) diffuses with increasing distance. No significant variation of the cross section is appreciable. We recall that we do not expect any focusing effect due to the fact that the entrance beam divergence is of the order of the crystallite Darwin width, as discussed before.

We have simulated the experiments described above with the ray tracing method described in Ref. 13. Fig. 6a shows the simulated focal spot for a mosaic crystal 1 mm thick with 0.25° mosaicity. The simulation shows an enlargement of the focal spot in the plane perpendicular to the diffraction plane proportional to the added divergence $2\tau \sin\theta_B$.

The broadening in the focal spot produced by the beam penetration in the crystal bulk is related to the secondary extinction coefficient. To study that, used the unfocused beam at 18 keV and recorded beam cross section in the proximity of the mosaic crystal. Some experimental beam profiles together with a ray tracing simulation are shown in Fig. 6b. We used a narrow incident beam (40 μm) defined by the entrance slit. The experimental results show some important facts: i) the beam profiles decay exponentially, with a measured mean free path (MFP) λ_{exp} which is the projection on the image plane of the MFP inside the crystal λ_{sec} due to the secondary extinction: $\lambda_{exp} = \lambda_{sec}/\sin(2\theta_B)$, ii) intensity irregularities are observed in some profiles due to macrostructures, and iii) the calculated MFP is of the order of the experimental ones. Work is in progress to analyze the images to obtain accurate values of MFP, secondary extinction coefficients and mosaicities.

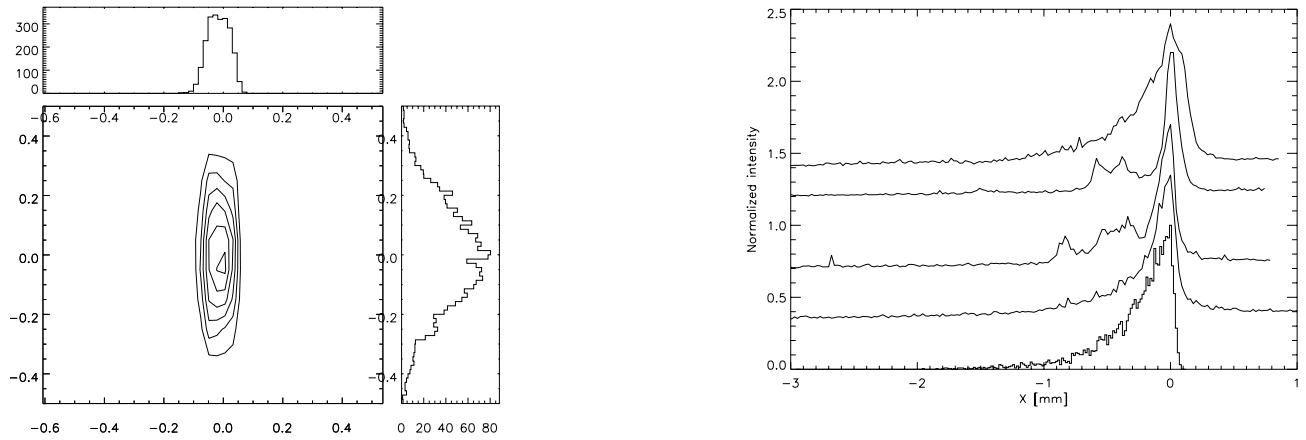

Figure 6. *Left:* Ray tracing simulations of the diffraction image 200 cm downstream of the mosaic crystal using the primary source. Units are cm. The calculated dimensions FWHM are 0.97 mm (H) and 4.95 mm (V). This graph can be compared with Fig. 5e.
Right: Diffracted beam cross section in the diffraction produced by a mosaic crystal using a narrow 40 μm collimated incident beam of 18 keV. The experimental profiles are obtained from measured images. From top to bottom: i) Panasonic sample, ii) Advanced Ceramics sample, iii) Optigraph (1.0 mm-thick) sample, iv) Optigraph (0.5 mm-thick) sample and, v) ray tracing simulation with a 1 mm thick mosaic crystal of τ=0.25°. Exponential fits of these curves gave the following MFP values: i) 0.33 mm, ii) 0.11 mm, iii) 0.27 mm, iv) 0.23 mm, and v) 0.32 mm. The resulting secondary extinction MPF vales (calculating the ratio between these values and $\sin(2\ \theta_B)$) are: i) 1.61 mm, ii) 0.54 mm, iii) 1.32 mm, iv) 1.12 mm, and v) 1.56 mm.

3.2. Beam evolution using the secondary source (focused beam)

The second experimental configuration used the sagittal focusing of the Si monochromator. As discussed above, the focus produced by the sagittally bent crystal of the monochromator has been used as a source for the mosaic crystal

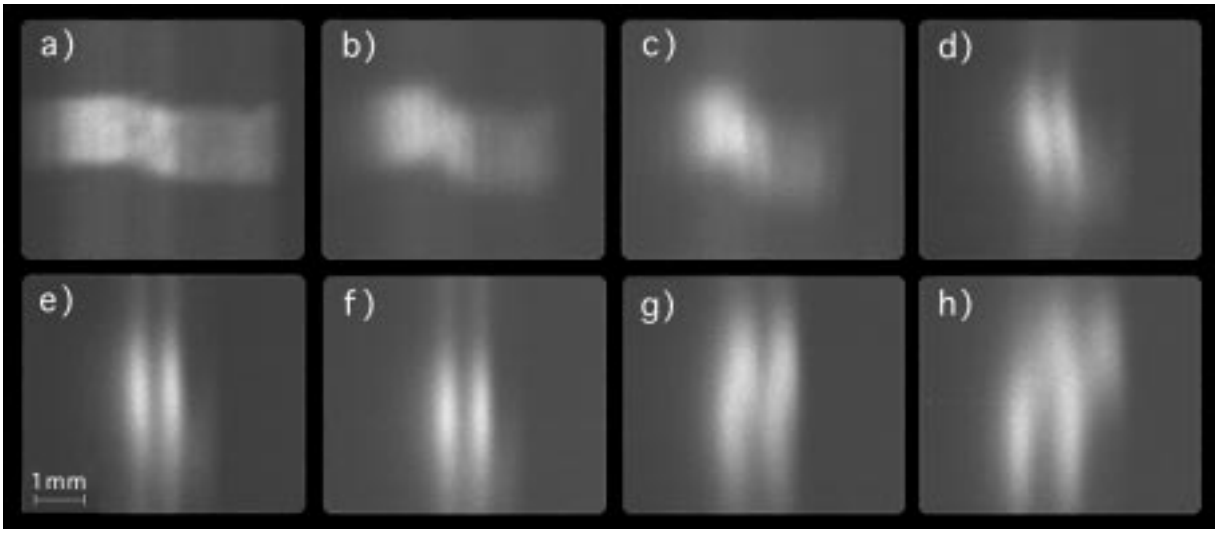

Figure 7. Radiographs of the beam cross section imaged with the digital detector at various distances downstream from the mosaic crystal: a) 20 cm, b) 40 cm, c) 60 cm, d) 80 cm, e) 96 cm (focus), f) 100 cm, g) 120 cm and h) 140 cm.

(secondary source) which has been experimentally found at 96 cm upstream from the mosaic crystal. The secondary source dimensions were defined by a slit (0.08 mm in horizontal and 1.5 mm in vertical). The selected energy of the monochromator was 18 keV. A set of images were recorded with the CCD at distances of 20, 40, 60, 80, 96, 100, 119 and 140 cm from the mosaic crystal. The images of the beam cross section are shown in Fig. 7. From these images it is clear that the horizontal beam decreases as the distance from the crystal is increased. This is the parafocusing effect. The minimum horizontal size found in these images corresponds to the expected position (96 cm from the mosaic crystal, verifying the 1:1 focusing). The horizontal beam cross section becomes larger downstream from this position.

These images show an unexpected result: a double focal spot always appears at the focal position. The double-spot is probably due to the existence of spatial structures in the incoming beam produced by the sagittal focusing. The surface imperfections (error in shape, which is not exactly cylindrical, and probably consists in two or more overlapped cylinders) and a possible misalignment produced spatial structures in the incoming beam to the mosaic crystal. The structures in the incident beam have been observed experimentally in several images around the focal position of the sagittal crystal (see Fig. 4).

The parafocusing effect was also investigated by the radiographs of a high-contrast test object. A bar pattern of 2 lp/mm was placed at 8.1 cm downstream from the mosaic crystal, and four images were recorded at 20, 40, 50, and 60 cm downstream from the mosaic crystal. All the images are reported in Fig. 8. The separation between maxima has been measured for the various images and the convergence of the beam obtained by fitting the experimental data. The linear fit (correlation factor 0.999) is shown below:

$$y = 0.551 - 0.00584\, x, \tag{2}$$

where y is the separation between maxima and x is the distance from the crystal, both in cm. The focal position resulted at 94 ± 2 cm from the mosaic crystal, thus confirming within the experimental error the expected results of 1: 1 focusing.

Several images of the focal spot produced by the mosaic crystals were recorded for different samples described in Table 1. These images are in Fig. 9 and all of them show the double-spot structure mentioned. This proves that the double-structure was produced by the beam and not by the HOPG.

The width of the focal spot can be obtained from the beam profiles in Fig. 9 and is about 0.6 mm. The focal size is determined by three factors: i) the secondary source size, defined by the 0.08 mm slit, ii) the broadening due to

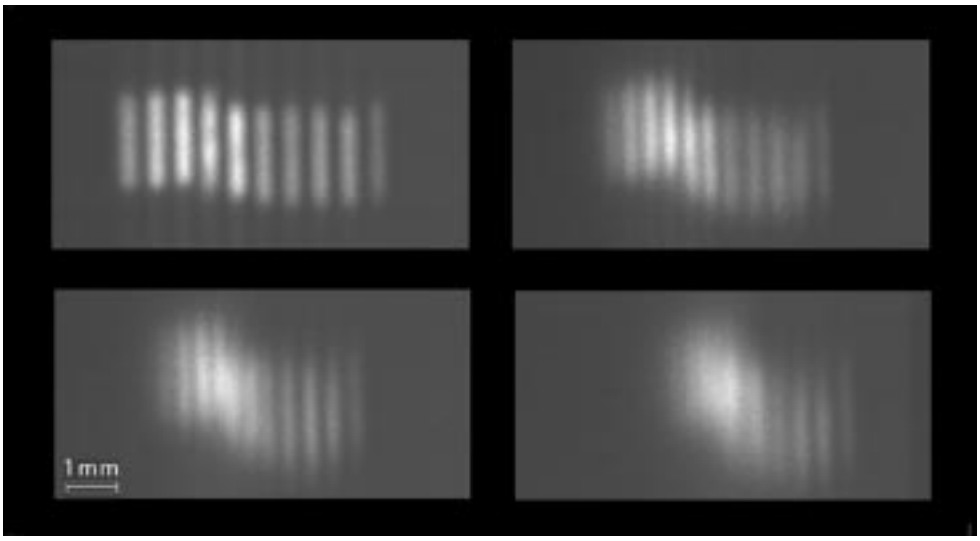

Figure 8. Radiographs of a 2 lp/mm bar pattern placed at 18 cm downstream from the mosaic crystal imaged with the digital detector at various distances (20, 40, 50 and 60 cm) from the mosaic crystal.

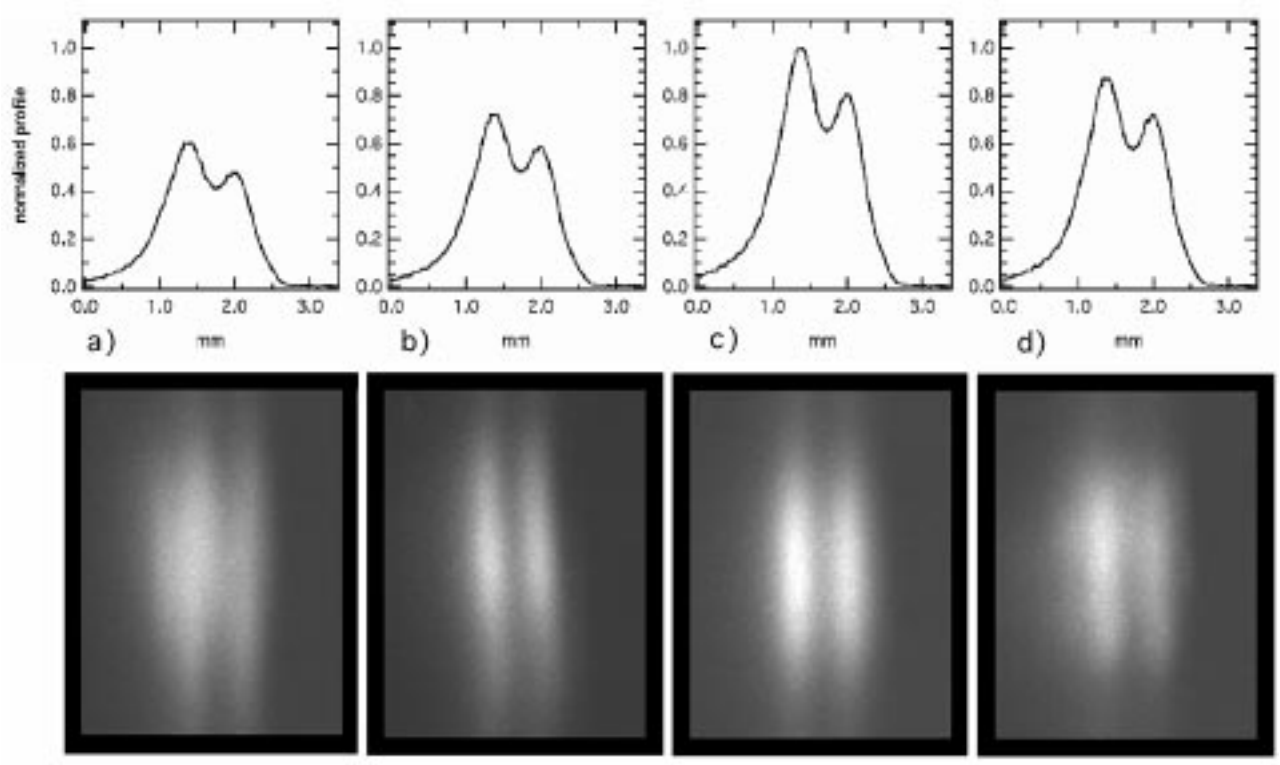

Figure 9. Images of the focal spot produced by the mosaic crystals obtained with the digital detector for different samples: a) Optigraph (0.5 mm-thick), b) Optigraph (1.0 mm-thick), c) Panasonic and d) Advanced Ceramics. The curves on the top of the figure are profiles taken in the center region of each bottom image.

the entrance beam energy bandwidth, which is negligible in our case ($\Delta E/E \approx 2\ 10^{-4}$ for the Si monochromator, giving an angular spread of $\Delta = (\Delta E/E)\tan\theta_B \approx 20\mu$ rad), and iii) the penetration of the beam inside the crystal bulk. The latter can be described by the secondary extinction coefficient, which for the case of ideal mosaic crystal can be written[7] as $\mu_s = W(\theta_B - \theta)\, Q$, being W the gaussian distribution of the crystallites and Q is proportional to the structure factor.

Fig. 10 shows a simulation for this setup and a 0.5 mm thick mosaic crystal of τ=0.25°. The resulting vertical focal size is 4.95 mm. Some simulations were also performed to confirm the hypothesis of the surface errors in the sagittal crystal. Fig. 11a shows the spot produced by a sagittal surface made by two overlapping cylinders of curvature radius 150 cm shifted by 0.04 mm with respect to the other (Fig. 11b).

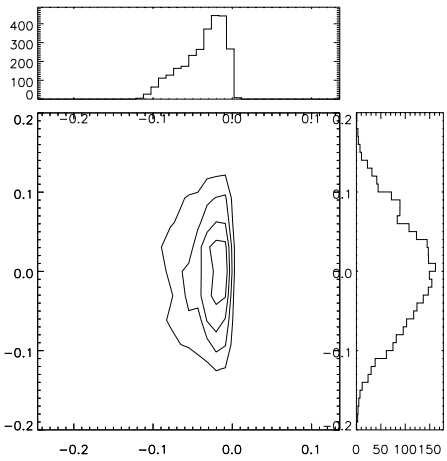

Figure 10. Simulation of the focal spot produced by a mosaic crystal that images the secondary source. Units are cm. Dimensions obtained from the FWHM of the histograms are 0.51 mm (H) and 1.75 mm (V). The mosaic crystal is 0.5 mm thick and has a mosaicity of τ=0.25°. This simulation can be compared with the experimental image in Fig. 9a.

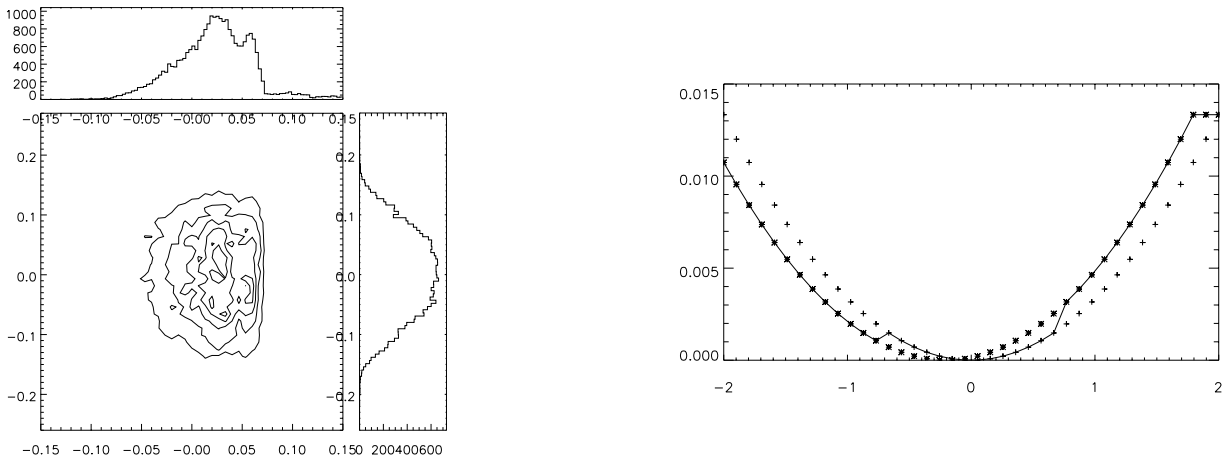

Figure 11. *Left:* ray tracing simulations of the focal spot produced by a mosaic crystal receiving monochromatic radiation (18 keV) focused with a sagittal crystal which surface is deformed. Units are cm.
Right: Profile of the sagittal surface (continuous line). It has been built by overlapping two cylindrical profiles (asteriscs and crosses) as explained in the text. Units are cm. The shifting dimensions are exaggerated for clarity.

4. SUMMARY AND CONCLUSIONS

The parafocusing effect of mosaic crystals (i.e. monochromatic focusing effect in the diffraction plane) was observed and measured experimentally. The focusing at the 1:1 (source-crystal and crystal-image) distance ratio was confirmed within the experimental errors. The defocusing effect in the plane perpendicular to the diffraction plane was also observed. The parafocusing was studied in samples from three different manufactures. An experimental setup to measure the secondary extinction coefficient was proposed and preliminary results were given. Work is in progress to improve the experimental layout in order to get quantitative data of the spot dimensions, that would give information related to the crystal mosaicity and perhaps macrostructure domains in HOPG. Imaging characteristics of these crystals are been evaluated by contrast images of bar-patterns compared with ray-tracing simulations.

ACKNOWLEDGMENTS

We acknowledge A. Souvorov and R. Tucoulou for their assistance during the experiment. Many thanks to M. Ohler for helpful discussions. Thanks also to P. Hoghoj and B. Hamelin for lending us the Panasonic crystal. We are indebted to I. Snigireva for supporting us with the ESRF Microimaging and Micromanipulation Laboratory. G.P. is grateful to the European Space Agency (ESA) to have financed a post-doctoral fellowship spent at the Danish Space Research Institute (Copenhagen, DK) during the period of this work.

REFERENCES

1. M. Gambaccini, A. Taibi, A. Del Guerra, F. Frontera and M. Marziani, "Narrow energy band x-rays via mosaic crystal for mammography application," *Nucl. Instr. and Meth.* **A365**, pp. 248–254, 1995.
2. M. Gambaccini, A. Taibi, A. Del Guerra and F. Frontera, "Small-field imaging properties of narrow energy band x-ray beams for mammography," *IEEE Trans. Nucl. Science* **43**, pp. 2049–2052, 1996.
3. F. Frontera and G. Pareschi, "Comparative study of hard X-ray (>10 keV) focusing techniques for space astronomy," *Proc. SPIE* **2515**, pp. 2–13, 1995.
4. F. Frontera and G. Pareschi, "Hard x-ray imaging via focusing optics with mosaic crystals," *Exper Astronomy* **6**, pp. 25–31, 1995.
5. A. K. Freund, "Mosaic crystals monochromators for synchrotron radiation instrumentation," *Nucl. Instr. and Meth.* **A266**, pp. 461–466, 1988.
6. A. K. Freund, "Application of mosaic crystals to high brilliance x-ray optics," *Proc. SPIE* **1740**, pp. 58–69, 1992.
7. W. H. Zachariasen, *Theory of x-ray diffraction in crystals*, Dover, New York, 1945.
8. G. E. Bacon and R. D. Lowde, "Secondary extinction and neutron crystallography," *Acta Cryst.* **1**, pp. 303–314, 1948.
9. A. K. Freund, "A tunable filter for reducing higher order contamination of monochromatic neutron beams," *Nucl. Instr. and Meth.* **A242**, p. 28, 1985.
10. A. K. Freund, A. Munkholm and S. Brennan, "X-ray diffraction properties of highly oriented pyrolithic graphite," *Proc. SPIE* **2856**, pp. 68–79, 1996.
11. M. Ohler, J. Baruchel, A. W. Moore, Ph. Galez and A. K. Freund, "Direct observation of mosaic blocks in highly oriented pyrolytic graphite," *Nucl. Instr. and Meth.* **B129**, pp. 257–260, 1997.
12. G. E. Ice and C. J. Sparks, "Mosaic crystal x-ray spectrometer to resolve inelastic background from anomalous scattering experiments," *Nucl. Instr. and Meth.* **A291**, pp. 110–116, 1990.
13. M. Sanchez del Rio, S. Bernstoff, A. Savoia and F. Cerrina, "A conceptual model for ray tracing calculations with mosaic crystals," *Rev. Sci. Instrum.* **63**, pp. 932–935, 1992.
14. M. Gambaccini, A. Del Guerra, A. Taibi and A. Tuffanelli, "Quasi-monochromatic x-ray source for mammography via crystal array," *Proc. SPIE* **3032**, pp. 154–160, 1997.
15. F. Frontera, P. De Chiara, G. Pareschi and G. Pasqualini, "Polarimetric performance of a bragg hard x-ray (>10 kev) concentrator," *Proc. SPIE* **2283**, pp. 85–93, 1994.
16. M. Gambaccini, A. Taibi, A. Del Guerra, M. Marziani and A. Tuffanelli, "MTF evaluation of a phosphor-coated CCD for x-ray imaging," *Phys. Med. Biol.* **41**, pp. 2799–2806, 1996.
17. A. Taibi, A. Del Guerra, M. Gambaccini, M. Marziani and A. Tuffanelli, "Evaluation of a digital x-ray detector based on a phosphor-coated CCD for mammography," *Nucl. Instr. and Meth.* **A392**, pp. 210–213, 1997.
18. M. Sanchez del Rio and R.J. Dejus, "XOP: Recent developments," *These Proc.* , 1998.